How to cite: *Angew. Chem. Int. Ed.* **2021**, *60*, 20498 – 20503
International Edition: doi.org/10.1002/anie.202107848
German Edition: doi.org/10.1002/ange.202107848

OLEDs

Multi-Resonance Deep-Red Emitters with Shallow Potential-Energy Surfaces to Surpass Energy-Gap Law**

Yuewei Zhang, Dongdong Zhang, Tianyu Huang, Alexander J. Gillett, Yang Liu, Deping Hu, Linsong Cui, Zhengyang Bin, Guomeng Li, Jinbei Wei, and Lian Duan**

Abstract: *Efficient organic emitters in the deep-red region are rare due to the "energy gap law". Herein, multiple boron (B)- and nitrogen (N)-atoms embedded polycyclic heteroaromatics featuring hybridized π-bonding/ non-bonding molecular orbitals are constructed, providing a way to overcome the above luminescent boundary. The introduction of B-phenyl-B and N-phenyl-N structures enhances the electronic coupling of those para-positioned atoms, forming restricted π-bonds on the phenyl-core for delocalized excited states and thus a narrow energy gap. The mutually ortho-positioned B- and N-atoms also induce a multi-resonance effect on the peripheral skeleton for the non-bonding orbitals, creating shallow potential energy surfaces to eliminate the high-frequency vibrational quenching. The corresponding deep-red emitters with peaks at 662 and 692 nm exhibit narrow full-width at half-maximums of 38 nm, high radiative decay rates of ca. $10^8\ s^{-1}$, ≈100% photoluminescence quantum yields and record-high maximum external quantum efficiencies of ca. 28% in a normal planar organic light-emitting diode structure, simultaneously.*

Introduction

The energy gap law,[1] recognized as the fact that non-radiative transitions will significantly increase with the decreased energy gap, has created a formidable barrier to produce deep-red (DR)/ near-infrared (NIR) organic emitters with high photo-luminescence quantum yields (PLQYs), despite their great demand for applications in night vision displays, biomedical imaging, optical communications and computing.[2] This effect is strong even for rigid systems, as was observed in the nonradiative deactivation of polycyclic aromatic hydrocarbons (PAHs).[3] In those large conjugation PAH structures, the highest occupied and lowest unoccupied molecular orbitals (HOMO and LUMO, respectively) are primarily localized between atoms, forming π-bonds with bonding/antibonding character. The resulted interactions between the electronic and nuclear vibrational motion will induce significant C=C torsion or C–H vibration with high frequency, forming deep potential energy surfaces (PES) as illustrated in Figure 1 a. In the absence of a zero-order surface crossing, such deep PES will facilitate the wavefunction overlap of the zero-vibration level (v_0) of the excited state (singlet or triplet, that is S_1 or T_1) and the high isoenergetic vibration level (v_n) of the ground state (S_0), consequently relaxing the excited states in a nonradiative decay pathway. For DR/NIR emitters with emission peaks >650 nm, the small energy gap between v_0s ($\Delta Ev_{0\text{-}0}$) of S_1 (or T_1) and S_0 will

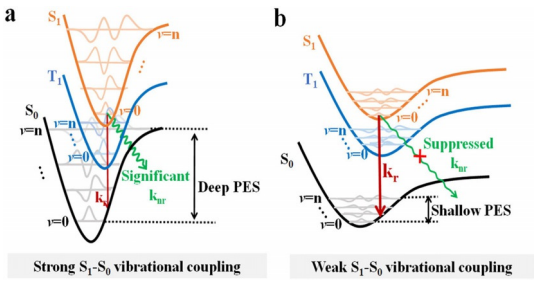

Figure 1. a) Scheme of excited states decay processes of PAHs with π-bonding and deep PES. b) Scheme of excited states decay processes of MR TADF emitters with non-bonding and shallow PES.

[*] Y. Zhang, Dr. D. Zhang, T. Huang, G. Li, Prof. L. Duan
Key Lab of Organic Optoelectronics and Molecular Engineering of Ministry of Education, Department of Chemistry, Tsinghua University
Beijing 100084 (P. R. China)
E-mail: ddzhang@mail.tsinghua.edu.cn
duanl@mail.tsinghua.edu.cn
Y. Zhang, Prof. L. Duan
Center for Flexible Electronics Technology, Tsinghua University
Beijing 100084 (P. R. China)
Dr. A. J. Gillett, L. Cui
Cavendish Laboratory, University of Cambridge
JJ Thomson Avenue, Cambridge CB3 0HE (UK)
Dr. Y. Liu, Z. Bin
Key Lab of Green Chemistry and Technology of Ministry of Education, Sichuan University
29 Wangjiang Road, Chengdu 610064 (P. R. China)
Dr. D. Hu
School of Environment, South China Normal University
Guangzhou 510006 (P. R. China)
Dr. J. Wei
Beijing National Larboratory for molecular Sciences, Insititute of Chemeistry, Chinese Academy of Sciences
Beijing 100190 (P. R. China)

[**] A previous version of this manuscript has been deposited on preprint servers (https://doi.org/10.26434/chemrxiv.13202975; https://doi.org/10.21203/rs.3.rs-119314/v1).

Supporting information and the ORCID identification number(s) for the author(s) of this article can be found under: https://doi.org/10.1002/anie.202107848.

exponentially accelerate this nonradiative transitions since only a few vibrational ladders in S_0 are required to satisfy the energy requirement for vibrionic coupling with v_0 of excited states, drastically reducing the emission intensity.[4]

Breakthroughs to surpass energy gap law have been made in planar platinum (Pt) complexes with dimers or oligomers to increase the exciton delocalization length, which can decouple the exciton band from high vibrational ladders in S_0 state and thus suppress nonradiative transitions.[5] This conceptually advancements in molecular design leads to NIR-emitters with impressive PLQYs of over 80% under emission peaks of 740 nm and high performance NIR organic light-emitting diodes (OLEDs). Recently, DR/NIR thermally activated delayed fluorescence (TADF) emitters with PLQYs > 80% and peaks at ≈650 nm have also been reported.[6] Determined by the onset of their wide emission spectra, the relatively larger $DEv_{0\text{-}0}$s of TADF emitters than PAHs with similar emission peaks are beneficial for suppressing the nonradiative transitions, though at the cost of the color purity. On the other hand, the charge transfer features of TADF emitters would always lead to large reorganization energies (λs) due to the large structure relaxation and thus much smaller radiative decay rates (k_rs) than that of PAHs. Therefore, it remains challenging to develop high color purity DR/NIR emitters with PLQYs up to 100%.

Recently, a new class of boron (B)- and nitrogen (N)-atoms embedded PAHs have been reported by Hatakeyama et al, in which the ortho-positioned electron donating N-atom and electron deficient B-atom induce complementary multiple resonance (MR) effects for the offset electron density distributions of HOMO and LUMO orbitals by one atom in an alternating pattern.[7] Such MR emitters not only inherit the merits of small λs of PAHs for high k_rs, but also minimizes the bonding/antibonding character between adjacent atoms. The so-called non-bonding character could significantly lower the vibration frequency in the molecules, leading to shallow PES of S_0 and S_1 states. In this regard, emitters with sharp photo-luminescence (PL) and electro-luminescence (EL) emissions can be expected. From another perspective, as illustrated in Figure 1b, for such shallow PES, more vibrational ladders in S_0 are required to reach the vibrionic coupling with v_0 of S_1 state, which is almost prohibited owing to their non-bonding characters, even for DR/NIR emitters. As a result, the high-frequency vibrational quenching can be theoretically eliminated in well-designed MR emitters, providing a way to surpass the energy gap law (Figure S1; Tables S1 and S2). Another bonus is that the alternated distributions of HOMO and LUMO render small energy gaps (ΔE_{ST}s) between S_1 and T_1 levels in these compounds and thus efficient TADF emissions.

Results and Discussion

For organic emitters, extending the π-conjugation length is an effective way to redshift the emission. The non-bonding characters in MR-TADF emitters, however, would limit the increasement of conjugation even with enlarged planar structures, making it challenging for DR/NIR emission.[7a,d] Enhancing the CT character in MR-TADF emitters is an alternative way to achieve redshifted emissions, which however, would weaken the MR effect and thus broadening the emission spectra.[7f] Quite recently, Yasuda and co-workers introduced a potential solution, that is, constructing two para-position boron atoms and two nitrogen atoms in the central π-core to significantly increase the acceptor and donor strengths.[7k] Consequently, a pure red emitter with emission peak at 615 nm was obtained. However, to the best of our knowledge, no DR/NIR MR emitter has ever been reported until now though being highly desired. To fulfill the requirement of narrowband DR/NIR emission, a multiple B and N atoms embedded polycyclic heteroaromatic motif was further proposed here, enabling multiple B and N centers and the modulation of their arrangement around a central phenyl ring. As illustrated in Figure 2a, besides the mutually ortho-positioned B and N atoms, which is the basic requirement for MR effect, multiple linear B-phenyl-B and N-phenyl-N structures were adopted. Previous works have demonstrated the formation of intramolecular dimeric radical between donors (or acceptors) in para positions due to the enhanced electronic coupling between a cation (or an anion) and a neutral moiety in linearly position.[8] The resulted delocalized excited states will significantly narrow energy gap and thus facilitating red-shifted emission.

Considering the features of small ΔE_{ST}, high oscillator strengths (fs) and minor λs of MR-TADF emitters, highly correlated SCS-CC2 calculations were adopted here.[7l–m] As expected, small S_1 values of 2.07 eV and 1.94 eV for R-BN and R-TBN were obtained here (Table S3). In contrast to TD-DFT, SCS-CC2 calculations on DtBuCzB, R-BN and R-TBN provide ΔE_{ST} values in excellent agreement with experiments (0.11 eV for DtBuCzB, 0.18 eV for R-BN and 0.17 for R-TBN, respectively, Figures S5,6 and Tables S3,4).[7g] It was interesting to note that on the central phenyl ring, both

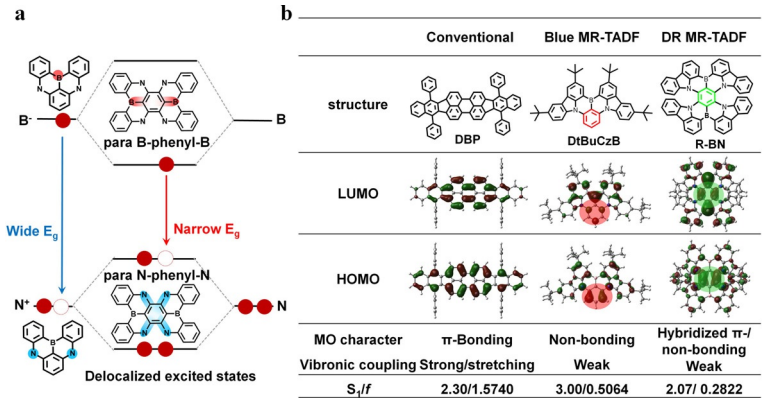

Figure 2. a) Scheme of the formation of delocalized excited states with B-phenyl-B and N-phenyl-N structures. b) The differences between conventional PAH (taking 3,8,13,18-tetraphenylbenzo[5,6]indeno[1,2,3-cd]benzo[5,6]indeno[1,2,3-lm]perylene (DBP) as an example), MR-TADF emitters with (taking DtBuCzB as an example) and without B-phenyl-B and N-phenyl-N structures.

HOMO and LUMO showed π-bond characters (Figure 2b and Figure S5), which arises from the coupling of electrons on para-positioned N atoms or B atoms as described above. The mutually ortho-positioned B and N atoms, meanwhile, induce MR effect on the peripheral skeleton, leading to the localization and separation of the HOMO and LUMO on different atoms. These non-bonding characters facilitate to lower vibration frequency for shallow PES in molecules as aforementioned and thus eliminate nonradiative transitions. The targeted emitters with hybridized π-bonding/ nonbonding molecular orbitals thereof possess the potential to fundamentally overcome the luminescent boundary set by the energy gap law. Additionally, the geometric changes of molecular conformation between S_0 and S_1 states and structural relaxation at the S_1 state are extremely small with reorganization (λ_S)/structural relaxation (λ_S*) energies were calculated to be merely 0.08 and 0.12 eV, 0.08 and 0.14 eV for R-BN and R-TBN, respectively (Figures S2–S4), significantly smaller than typical DR/NIR organic molecules (0.26–0.52 eV).[5b,9] Those extremely small λ_S and λ_S* facilitate narrow bandwidth emission with high radiative transitions and high oscillator strength (*f*) values of 0.34 and 0.37 for R-BN and R-TBN were obtained, respectively (Table S3).

R-BN and R-TBN were synthesized in two steps from commercially available starting materials and no palladium or other transition metal catalysts were needed, making them cost effective. The single crystal X-ray diffraction analyses shows that R-BN/R-TBN is a special double helix structure composed of two fused screw structures, where small torsional angles (≈20°) of the carbazolyl groups could be found (Figure 3a and Figure S7). This limited torsional flexibility can be another major factor in reducing the non-radioactive decay of R-BN/R-TBN. Photophysical properties of R-BN and R-TBN in toluene with a concentration of 10^{-5} M were measured and listed in Table 1. Strong absorption bands with a maximum at 629 nm ($\log\varepsilon = 4.73$, where ε is the molar excitation coefficient) and 651 nm ($\log\varepsilon = 4.82$) were recorded for R-BN and R-TBN, respectively (Figure 3b and Figure S8). Arising from the small optical energy gaps of 1.87 eV and 1.79 eV for R-BN and R-TBN, deep red fluorescence emission peaked at 662 nm and 692 nm were observed. Moreover, a much larger S_1 energy of 2.66 eV was found in BBCz-DB molecules, which possessed a similar structure with multiple B, N atoms but not linear N-phenyl-N and B-phenyl-B, suggesting the N-phenyl-N and B-phenyl-B structure motif is essential for the formation of delocalized excited states.[7g] The PLQY increased from 90% (R-BN)/ 88% (R-TBN) to 100% after 10 min of N_2 bubbling to remove the dissolved oxygen, suggesting that the triplet states formed through ISC process can be recycled. Their small full-width at half-maximums (FWHMs) of both 38 nm reflect the narrow energy bandwidths of both S_0 and S_1 states as illustrated in Figure 1b and thus the minimized the vibronic coupling between the S_0 and S_1 states. Also, small stokes shifts of 33 nm and 41 nm were also exhibited for R-BN and R-TBN, respectively, suggesting the limited vibrational relaxation at the S_1 state. All those parameters combined to overcome the limitation of energy gap law as aforementioned.

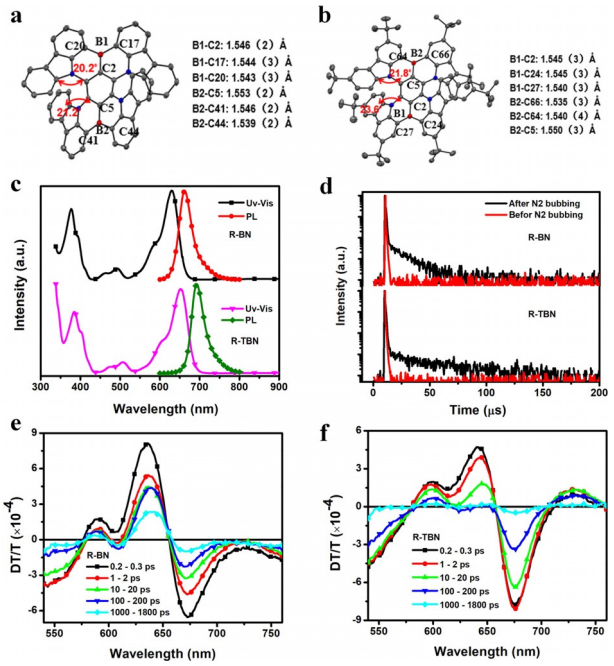

Figure 3. ORTEP drawings of R-BN (a) and R-TBN (b) obtained by X-ray crystallographic analysis. Thermal ellipsoids are shown at 50% probability. Hydrogen atoms are omitted for clarity. c) UV/Vis absorption and fluorescence (298 K) spectra of R-BN and R-TBN in toluene. d) Transient PL decay curves of R-BN and R-TBN in toluene solution before (red) and after (black) N_2 bubbling for 10 min. Transient absorption (TPA) spectra of R-BN (e) and R-TBN (f) doped in PMMA films (3 wt%) at room temperature.

The triplet energies were obtained from phosphorescent spectra recorded in a frozen toluene (77 K) matrix with a delay time of 10 ms, being 1.69 eV and 1.63 eV for R-BN and for R-TBN, respectively (Figure S9). The corresponding ΔE_{ST} values were 0.18 eV for R-BN and 0.16 eV for R-TBN. Such small ΔE_{ST} values are favorable for exciton up-conversion from T_1 to S_1 at ambient condition. Transient PL decay curves before and after N_2 bubbling and the detailed analyses are provided in Figure 3b and Table S5. Both prompt (τ_F =

Table 1: Summary of the photophysical properties of R-BN and R-TBN.

	S_1[a] [eV]	T_1[a] [eV]	ΔE_{ST}[a] [eV]	FWHM[a] [nm]	HOMO[b] [eV]	LUMO[c] [eV]	PLQY[a]	τ_{PF}[a] [ns]	τ_{DF}[a] [μs]	k_r[a] [$\times10^7$ s^{-1}]	k_{ISC}[a] [$\times10^6$ s^{-1}]	k_{RISC}[a] [$\times10^4$ s^{-1}]
R-BN	1.87	1.69	0.18	38	−4.76	−3.06	100%	12.0	16.6	7.5	8.3	6.7
R-TBN	1.79	1.63	0.16	38	−4.69	−3.00	100%	14.2	46.4	6.2	8.5	2.5

[a] Measured in the deoxygenated toluene solution with a concentration of 10^{-5} mol L^{-1}. [b] Determined from the half-wave potentials of the oxidation curves in dry dichloromethane with a concentration of 10^{-3} mol L^{-1}. [c] Determined from the half-wave potentials of the reduction curves in dry N,N-dimethylformamide with a concentration of 10^{-3} mol L^{-1}.

12.0 ns for R-BN and 14.2 ns for R-TBN) and delayed fluorescence ($\tau_{DF} = 16.6$ μs and $\tau_{DF} = 46.4$ μs for R-BN) components were clearly identified in deoxygenated toluene solutions, which can be unambiguously assigned to the TADF emission. The values of the rate constants of fluorescence (k_r), intersystem crossing (k_{ISC}), reverse intersystem crossing (k_{RISC}) and nonradiative transition (k_{nr}) were calculated to be 7.5×10^7, 8.3×10^6, 6.7×10^4 s^{-1}, and $<7.5\times10^4$ s^{-1} for R-BN, 6.2×10^7, 8.5×10^6, 2.5×10^4 s^{-1} and $<6.2\times10^4$ s^{-1} for R-TBN, respectively, using the new methodology provided in the literature.[10] The large k_r values are consistent with the large molar excitation coefficient ($\log\varepsilon = 4.73$ for R-BN and 4.82 for R-TBN, respectively) and large oscillator strengths. Compared to those of donor-acceptor ICT-type TADF emitters, the k_{RISC} values of R-BNs were relatively low ($\approx10^3$ s^{-1}) because their ΔE_{ST} values (180/160 meV) were much larger than the thermal energy at 300 K ($k_{BT} \approx 25.9$ meV). To the best of our knowledge, an inefficient RISC process is a common issue for MR-TADF emitters.

The photophysical properties of R-BN/R-TBN in the form of a thin film (3 wt%-doped in 4,4′-di(9H-carbazol-9-yl)-1,1′-biphenyl (CBP)) were also measured. High PLQYs of unity were maintained for both films though their significantly redshifted emission peaking at 672 nm and 698 nm for R-BN and R-TBN, respectively, suggesting the strong ability of those molecules in beating the limitation of energy gap law (Figure S11). Also, a relatively larger FWHMs of 48 nm and 49 nm were recorded for R-BN and R-TBN compared with the ones in solution, respectively, partly attributed to the interaction between host and dopant, which has been pointed out in previous works.[7a] Their transient PL decay characteristics were also examined (Figure S12), revealing obvious TADF features with short-lived prompt and long-lived delayed components ($\tau_F = 4.7$ ns and $\tau_{DF} = 0.31$ ms for R-BN, $\tau_F = 10.3$ ns and $\tau_{DF} = 0.71$ ms for R-TBN). These are promising characteristics of TADF dyes for their application as emission layers in OLEDs.

To gain further insight into the nature of electronic excited states, femtosecond pump-probe transient absorption (TA) measurements for R-BN and R-TBN in doped films (3 wt% in poly(methyl methacrylate)) were carried out. As shown in Figures 3e,f, both TA spectra of R-BN and R-TBN showed broad excited-state absorption (EAS) signals, overlapping with two ground state bleach (GSB) bands as well as a stimulated emission (SE) band. Specifically, for R-TBN in doped film, the SE signal at 735 nm rises rapidly and then decay after 3 ps, along with the 675 nm ESA signal decay quickly, corresponding to the vibrational relaxation process from the high vibration levels of S_1 state to the zero-vibration level of the S_1 state, and then undergo an ultrafast radiative process within 1.8 ns, in line with its high k_r and PLQY mentioned above. On the other hand, during the following 0.2–10 ps, the $S_0 \rightarrow S_1$ GSB signal around 640 nm exhibited a neglectable peak shift from 641 nm to 645 nm, corresponding to the depopulation of excitons on the vibrational states. This also evidences that both R-BN and R-TBN possess shallow potential energy surface, resulting in the narrow bandwidth emission.

OLEDs were further constructed to evaluate the performances of those two emitters with the following structures of Indium tin oxide (ITO) / 1,4,5,8,9,11-hexaazatriphenylene hexacarbonitrile (HATCN, 10 nm) / 1,1-bis[(di-4-tolylamino)phenyl]cyclohexane (TAPC, 70 nm) / tris(4-carbazolyl-9-ylphenyl)amine (TCTA, 10 nm) / EMLs (25 nm) / 4,6-bis(3-(9H-carbazol-9-yl)phenyl)pyrimidine (CzPhPy, 10 nm) / 4,6-Bis(3,5-di(pyridin-4-yl)phenyl)-2-methylpyrimidine (B4PyMPM, 45 nm) / LiF (0.5 nm) / Al (150 nm). Considering the relatively long delayed fluorescence lifetimes of these two emitters, the EMLs adopt a ternary system of CBP: 30 wt% Ir(mphmq)$_2$tmd: 3 wt% R-BN/R-TBN, where Ir(mphmq)$_2$tmd was used as the phosphorescence sensitizer to assist the exciton recycle under electrical excitation.[11] The sensitized emission process was provided in Figure S13 with detailed analysis. The device energy levels were provided in Figure 4a. Electro-luminance spectra with peaks at 664 nm and 686 nm were recorded for R-BN and R-TBN based devices with small FWHMs of 48 nm and 49 nm as illustrated in Figure 4b, leading to CIE coordinates of (**0.719**, 0.280) and (**0.721**, 0.278), respectively. The CIE$_x$ here outperforms all reported values of DR TADF emitters with even red-shifted emission peaks benefiting from their narrow emission bandwidth.[2b,6,12] For deep red emitters, the radiance is also an important parameter to evaluate their brightness. Maximum radiance of 6.4×10^5 mW sr^{-1} m^{-2} for R-BN and 7.1×10^5 mW sr^{-1} m^{-2} for R-TBN devices were recorded as depict-

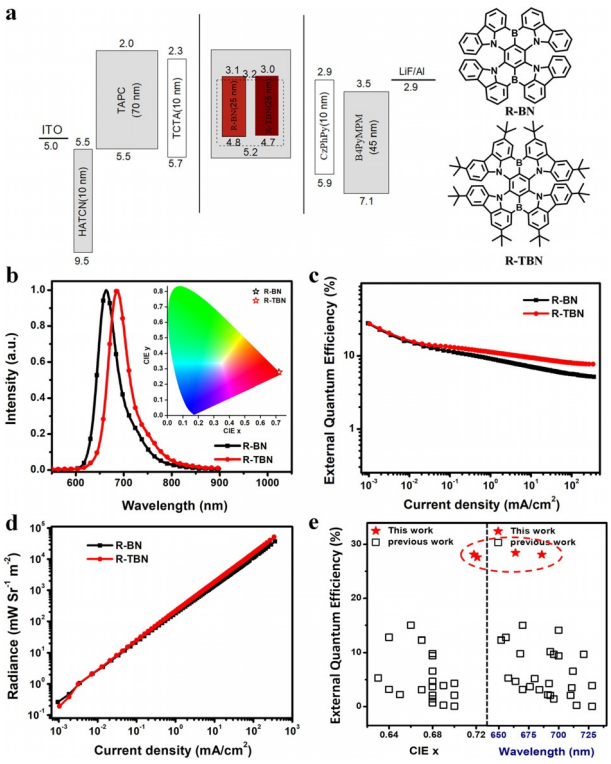

Figure 4. a) The energy-level diagrams and the emitter structures of the devices. b) The EL spectra of the optimized DR/NIR devices. c) EQE versus current density characteristics. d) Radiance versus current density characteristics. e) CIE *x* (left)/EQE (right) summary of DR/NIR TADF-OLEDs with emission peak >650 nm (for references, see Table S5, Supporting Information).

ed in Figure 4c. Unprecedently high maximum EQEs of 28.1 % and 27.6 % were observed for R-BN and R-TBN based devices (Figure 4d), respectively. As revealed in Figure 4e, to the best of our knowledge, these values are not only the highest records among all reported results of devices using TADF emitters with peaks >650 nm,[2b,6,12] but also comparable to the most efficient DR/NIR PHOLEDs (circa 24 %) with similar spectra.[5a,13] Furthermore, the lifetimes of the unpackaged devices were testified, showing decent T90s (times of luminance decay to 90 % of the initial one) of 125 h and 151 h, respectively, under an initial luminance of 2000 cd m^{-2} (Figure S18). Those decent lifetimes testify the stability of those emitters.

The basic device performance of R-BNs was also investigated using CBP: R-BN and CBP: R-TBN emitting layers, of which the maximum EQEs could still maintain 25.6 % and 24.7 % for R-BN and R-TBN, respectively (Figures S19–21 and Tables S7,8). Devices with and without phosphor sensitizers showed identical EL spectra, suggesting the complete energy transfer in the sensitized devices. Those unprecedently high performances obtained here testify the great potential of the molecular design strategy. However, those devices exhibited significant efficiency roll-off, partly attributed to the inefficient RISC process of those R-BNs. And we believed that by further optimizing device structures, the EL performances of those emitters may be further improved.

Conclusion

Efficient and bright DR/NIR MR-TADF emitters derived from multiple boron (B) and nitrogen (N) atoms embedded polycyclic heteroaromatics were developed to fundamentally overcome the luminescent boundary set by the "energy gap law". By adopting B-phenyl-B and N-phenyl-N structures with mutually ortho-positioned B and N atoms, hybridized π-bonding/ nonbonding molecular orbitals are recorded, not only narrowing energy gap for DR/NIR emission by the delocalized excited states but also eliminating nonradiative transitions by suppressing vibration coupling due to the shallow potential energy curve induced by MR effect. Deep red emitters showed high PLQYs of ≈ 100 % and maximum EQE of ≈ 28 % with narrow bandwidth emission spectra. This work here provides a strategic implementation of multiple B and N atoms in polycyclic heteroaromatics, showing viable potential to generate DR/NIR emitters with bright and efficient emission without nonradiative transitions. Also, what should be further stressed is that owing to the narrow bandwidth emission, DR/NIR MR-TADF emitters usually exhibit extremely high k_rs, which is indispensable to lower the amplified spontaneous emission (ASE) thresholds in organic DR/NIR lasers.

Acknowledgements

This work was supported by the National Key Basic Research and Development Program of China (Grant No. 2020YFA0715000), the National Science Fund of China (Grant Nos. 51903137, and 61890942), the China Postdoctoral Science Foundation (Grant No. 2019M650628), the Guangdong Major Project of Basic and Applied Basic Research (Grant No. 2019B030302009) and Foshan Xianhu Laboratory of the Advanced Energy Science and Technology Guangdong Laboratory XHT2020-005.

Conflict of Interest

The authors declare no conflict of interest.

Keywords: energy gap law · hybridized π-bonding/ non-bonding orbitals · OLEDs · polycyclic heteroaromatics · shallow potential energy surfaces

[1] a) J. V. Caspar, T. J. Meyer, *J. Phys. Chem.* **1983**, *87*, 952 – 957; b) J. V. Caepar, E. M. Kober, B. P. Sullivan, T. J. Meyer, *J. Am. Chem. Soc.* **1982**, *104*, 630.

[2] a) T. Yamanaka, H. Nakanotani, S. Hara, T. Hirohata, C. Adachi, *Appl. Phys. Express* **2017**, *10*, 074101; b) Y. Yuan, Y. Hu, Y.-X. Zhang, J.-D. Lin, Y.-K. Wang, Z.-Q. Jiang, L.-S. Liao, S.-T. Lee, *Adv. Funct. Mater.* **2017**, *27*, 1700986; c) N. Tessler, V. Medvedev, M. Kazes, S. Kan, U. Banin, *Science* **2002**, *295*, 1506; d) A. Antaris, H. Chen, K. Cheng, Y. Sun, G. Hong, C. Qu, S. Diao, Z. Deng, X. Hu, B. Zhang, X. Zhang, O. Yaghi, Z. Alamparambil, X. Hong, Z. Cheng, H. Dai, *Nat. Mater.* **2016**, *15*, 235; e) D. Wang, M. M. S. Lee, G. Shan, R. T. K. Kwok, J. W. Y. Lam, H. Su, Y. Cai, B. Z. Tang, *Adv. Mater.* **2018**, *30*, 1802105.

[3] A. Zampetti, A. Minotto, F. Cacialli, *Adv. Funct. Mater.* **2019**, *29*, 1807623.

[4] a) W. Siebrand, *J. Chem. Phys.* **1967**, *47*, 2411; b) R. Englman, J. Jortner, *Mol. Phys.* **1970**, *18*, 145.

[5] a) K. T. Ly, R.-W. Chen-Cheng, H.-W. Lin, Y.-J. Shiau, S.-H. Liu, P.-T. Chou, C.-S. Tsao, Y.-C. Huang, Y. Chi, *Nat. Photonics* **2017**, *11*, 63; b) Y.-C. Wei, S. F. Wang, Y. Hu, L.-S. Liao, D.-G. Chen, K.-H. Chang, C.-W. Wang, S.-H. Liu, W.-H. Chan, J.-L. Liao, W.-Y. Hung, T.-H. Wang, P.-T. Chen, H.-F. Hsu, Y. Chi, P.-T. Chou, *Nat. Photonics* **2020**, *14*, 570.

[6] a) J. Xue, Q. Liang, R. Wang, J. Hou, W. Li, Q. Peng, Z. Shuai, J. Qiao, *Adv. Mater.* **2019**, *31*, 1808242; b) B. Zhao, H. Wang, C. Han, P. Ma, Z. Li, P. Chang, H. Xu, *Angew. Chem. Int. Ed.* **2020**, *59*, 19042; *Angew. Chem.* **2020**, *132*, 19204; c) T. Yang, B. Liang, Z. Cheng, C. Li, G. Lu, Y. Wang, *J. Phys. Chem. C* **2019**, *123*, 18585; d) J. Kumsampao, C. Chaiwai, P. Chasing, T. Chawanpunyawat, S. Namuangruk, T. Sudyoadsuk, V. Promarak, *Chem. Asian J.* **2020**, *15*, 3029.

[7] a) Y. Kondo, K. Yoshiura, S. Kitera, H. Nishi, S. Oda, H. Gotoh, Y. Sasada, M. Yanai, T. Hatakeyama, *Nat. Photonics* **2019**, *13*, 678; b) T. Hatakeyama, K. Shiren, K. Nakajima, S. Nomura, S. Nakatsuka, K. Kinoshita, J. Ni, Y. Ono, T. Ikuta, *Adv. Mater.* **2016**, *28*, 2777 – 2781; c) S. Nakatsuka, H. Gotoh, K. Kinoshita, N. Yasuda, T. Hatakeyama, *Angew. Chem. Int. Ed.* **2017**, *56*, 5087; *Angew. Chem.* **2017**, *129*, 5169; d) K. Matsui, S. Oda, K. Yoshiura, K. Nakajima, N. Yasuda, T. Hatakeyama, *J. Am. Chem. Soc.* **2018**, *140*, 1195 – 1198; e) X. Liang, Z.-P. Yan, H.-B. Han, Z.-G. Wu, Y.-X. Zheng, H. Meng, J.-L. Zuo, W. Huang, *Angew. Chem. Int. Ed.* **2018**, *57*, 11316 – 11320; *Angew. Chem.* **2018**, *130*, 11486 – 11490; f) J. A. Knöller, G. Meng, X. Wang, D. Hall, A. Pershin, D. Beljonne, Y. Olivier, S. Laschat, E. Zysman-Colman, S. Wang, *Angew. Chem. Int. Ed.* **2020**, *59*, 3156 – 3160; *Angew. Chem.* **2020**, *132*, 3181 – 3185; g) Y. Xu, Z. Cheng, Z. Li, B. Liang, J. Wang, J. Wei, Z. Zhang, Y. Wang, *Adv. Opt. Mater.* **2020**, *8*, 1902142; h) Y. Xu, C. Li, Z. Li, Q. Wang, X. Cai, J. Wei,

Y. Wang, *Angew. Chem. Int. Ed.* **2020**, *59*, 17442; *Angew. Chem.* **2020**, *132*, 17595; i) Y. Zhang, D. Zhang, J. Wei, Z. Liu, Y. Lu, L. Duan, *Angew. Chem. Int. Ed.* **2019**, *58*, 16912; *Angew. Chem.* **2019**, *131*, 17068; j) Y. Zhang, D. Zhang, J. Wei, X. Hong, Y. Lu, D. Hu, G. Li, Z. Liu, Y. Chen, L. Duan, *Angew. Chem. Int. Ed.* **2020**, *59*, 17499; *Angew. Chem.* **2020**, *132*, 17652; k) M. Yang, I. S. Park, T. Yasuda, *J. Am. Chem. Soc.* **2020**, *142*, 19468; l) A. Pershin, D. Hall, V. Lemaur, J. C. Sancho-Garcia, L. Muccioli, E. Zysman-Colman, D. Beljonne, Y. Olivier, *Nat. Commun.* **2019**, *10*, 597; m) D. Hall, S. M. Suresh, P. L. dos Santos, E. Duda, S. Bagnich, A. Pershin, P. Rajamalli, D. B. Cordes, A. M. Z. Slawin, D. Beljonne, A. Köhler, I. D. W. Samuel, Y. Olivier, E. Zysman-Colman, *Adv. Opt. Mater.* **2020**, *8*, 1901627.

[8] a) H. Noda, X. K. Chen, H. Nakanotani, T. Hosokai, M. Miyajima, N. Notsuka, Y. Kashima, J. L. Bredas, C. Adachi, *Nat. Mater.* **2019**, *18*, 1084 – 1090; b) D. Zhang, X. Song, A. J. Gillett, B. H. Drummond, S. T. E. Jones, G. Li, H. He, M. Cai, D. Credgington, L. Duan, *Adv. Mater.* **2020**, *32*, 1908355.

[9] G. R. Hutchison, M. A. Ratner, T. J. Marks, *J. Am. Chem. Soc.* **2005**, *127*, 2339 – 2350.

[10] Y. Wada, H. Nakagawa, S. Matsumoto, Y. Wakisaka, H. Kaji, *Nat. Photonics* **2020**, *14*, 643 – 649.

[11] a) K. H. Lee, J. Y. Lee, *J. Mater. Chem. C* **2019**, *7*, 8562 – 8568; b) J. H. Lee, H. Shin, J. M. Kim, K. H. Kim, J. J. Kim, *ACS Appl. Mater. Interfaces* **2017**, *9*, 3277.

[12] a) R. Furue, K. Matsuo, Y. Ashikari, H. Ooka, N. Amanokura, T. Yasuda, *Adv. Opt. Mater.* **2018**, *6*, 1701147; b) C. Li, R. Duan, B. Liang, G. Han, S. Wang, K. Ye, Y. Liu, Y. Yi, Y. Wang, *Angew. Chem. Int. Ed.* **2017**, *56*, 11525; *Angew. Chem.* **2017**, *129*, 11683; c) S. Wang, X. Yan, Z. Cheng, H. Zhang, Y. Liu, Y. Wang, *Angew. Chem. Int. Ed.* **2015**, *54*, 13068; *Angew. Chem.* **2015**, *127*, 13260; d) K. Sun, D. Chu, Y. Cui, W. Tian, Y. Sun, W. Jiang, *Org. Electron.* **2017**, *48*, 389; e) D.-H. Kim, A. D′Aléo, X.-K. Chen, A. D. S. Sandanayaka, D. Yao, L. Zhao, T. Komino, E. Zaborova, G. Canard, Y. Tsuchiya, E. Choi, J. W. Wu, F. Fages, J.-L. Brédas, J.-C. Ribierre, C. Adachi, *Nat. Photonics* **2018**, *12*, 98; f) J.-X. Chen, W.-W. Tao, W.-C. Chen, Y.-F. Xiao, K. Wang, C. Cao, J. Yu, S. Li, F.-X. Geng, C. Adachi, C.-S. Lee, X.-H. Zhang, *Angew. Chem. Int. Ed.* **2019**, *58*, 14660 – 14665; *Angew. Chem.* **2019**, *131*, 14802 – 14807; g) Y. M. Zhang, J. T. Wu, J. Song, Z. Chen, J. J. He, X. Wang, H. Y. Liu, S. M. Chen, J. L. Qu, W.-Y. Wong, *Adv. Electron. Mater.* **2019**, *5*, 1800677.

[13] M. Cocchi, J. Kalinowski, D. Virgili, J. A. G. Williams, *Appl. Phys. Lett.* **2008**, *92*, 113302.

Manuscript received: June 12, 2021
Version of record online: July 28, 2021

